Electron scattering from H_2^+: Resonances in the Σ and Π symmetries

L.A. Collins
T-Division, Los Alamos National Laboratory, Los Alamos, New Mexico 87545

B.I. Schneider
T-Division, Los Alamos National Laboratory, Los Alamos, New Mexico 87545
and Physics Division, National Science Foundation, Arlington, Virginia 22230

D.L. Lynch
Thinking Machines Corporation, 245 First Street, Cambridge, Massachusetts 02142

C.J. Noble
TCS Division, SERC Daresbury National Laboratory,
Daresbury, Warrington WA4 4AD, United Kingdom
(Received 18 July 1994; revised manuscript received 16 February 1995)

We present results of calculations for $e^- + H_2^+$ scattering in the energy regime below the first excited state for resonance symmetries Σ and Π. We employ three distinct and independent methods: close-coupling linear algebraic, effective optical potential linear algebraic, and R matrix. We report extended calculations on the $^1\Pi_g$ resonance, important to dissociative recombination. We show binding of the $^1\Sigma_g$ state resonance between 2.6 and 2.7 bohrs. Our $^1\Sigma_u$ state results agree very well with previous calculations and reside a factor of 2 below a recent experiment.

PACS number(s): 34.80.Gs

I. INTRODUCTION

In an earlier paper [1], we investigated the Π resonances for electron scattering from the hydrogen molecular ion H_2^+ below the first excited state (σ_u). We discovered interesting behavior of the lifetimes of the composite autoionizing states as a function of internuclear separation R. This behavior demonstrated the profound effects of channel coupling and interference of different resonant series. In addition, we compared three sophisticated computational methods in order to ascertain their efficacy, accuracy, and suitability for this case of strong channel coupling. The comparison demonstrated that all three techniques gave resonance parameters in very close agreement over a wide range of scattering conditions. We now extend these procedures to the Σ resonances by performing cross comparisons among the methods and by investigating the behavior of the resonance parameters as a function of R and various approximations. These parameters have important applications in a variety of processes [2,3] including dissociative recombination, dissociative photoionization, and associative ionization as well as to basic electron-molecule collisions [4–10]. Indeed, a recent experiment [11] predicts a $^1\Sigma_u$ resonant width far larger than obtained in previous theoretical treatments. In addition, such resonant states play important roles in the emerging areas of optimal coherent control [12] and molecules in intense electromagnetic fields [13]. Since a detailed history, complete with extensive citations, together with a thorough description of the methods appears in a prior paper [1], we shall concentrate principally on the Σ states and, as a matter of completeness, present some additional Π results. We begin with a short sketch of the basic formalism and of the computational procedures (Sec. II) and then discuss the results for the various resonant states (Sec. III).

II. FORMALISM

We employ three distinct techniques to explore electron collisions with H_2^+: the R matrix (RM), the close-coupling linear algebraic (CCLA), and the effective optical-potential linear algebraic (EOLA) methods. These methods have been successfully applied to a wide variety of molecular systems and processes [6,14]. We have demonstrated [1] for the Π resonances that they give remarkably accurate and consistent results for such sensitive parameters as the widths. In this section, we give only a schematic presentation of the techniques since extensive expositions appear elsewhere [1,4,6,10,14]. Atomic units apply throughout the paper unless otherwise noted.

The time-independent Schrödinger equation that describes the interaction of a continuum electron with the single-electron target molecule in the adiabatic-nuclei approximation has the form

$$H\psi(1,2) = E\psi(1,2), \tag{1}$$

$$H = H_0 + T_e + V_{ee} + V_{en}, \tag{2}$$

where V_{ee} is the interaction between the two electrons, V_{en} the interaction of an electron with the nuclear charge,

and T_e the kinetic energy of the colliding electron. The term H_0 represents the Hamiltonian for the H_2^+ molecule with eigensolutions of the form

$$H_0\varphi_n(1) = \epsilon_n\varphi_n(1). \tag{3}$$

At the equilibrium separation of 2.0 bohrs, the bound states have the following order: $1\sigma_g$, $1\sigma_u$, $1\pi_u^{\pm}$, $2\sigma_g$, $2\sigma_u$, $1\pi_g^{\pm}$, ..., while at larger R values, some of the higher σ states may intrude. We expand the total system wave function as

$$\psi(1,2) = \sum_{n=1}^{m} A[\varphi_n(1)F_n(2)] + \sum_a \chi_a(1,2)d_a \tag{4}$$

such that

$$(\varphi_n|F_{n'}) = 0, \tag{5}$$

where A represents an operator that forces the bound (φ_n) and the continuum (F_n) solutions to be properly antisymmetric. The orthogonality constraint is imposed for all n' in the RM and EOLA methods and for all $n' \neq n$ in the CCLA method. The essential difference between the two orthogonality constraints is the presence of additional one-electron terms in the CCLA approach. The first term (P space) represents the summation over a selected set of target states, usually those containing the desired scattering information, while the second term (Q space) appears for completeness. The L^2 expressions χ_a, termed correlation functions, must be introduced to relax the strong orthogonality constraint of Eq. (5). In addition, they are also capable of introducing correlation-polarization effects missing from P space. In all three approaches, we follow the general RM strategy and divide coordinate space into two regions. In the inner zone ($r \leq a$), we include the direct, the exchange, and the correlation effects through a solution of Eq. (1), subject to RM boundary conditions at $r = a$. To incorporate these boundary conditions directly into the Hamiltonian, we introduce a Bloch operator [15] $\mathcal{L}$ defined by

$$\mathcal{L} = \sum_j |\phi_j\rangle\delta(r-a)\left[\frac{\partial}{\partial r} - \frac{(b-1)}{r}\right]\langle\phi_j|, \tag{6}$$

where $|\phi_j\rangle$ is a channel function and b is the value of the logarithmic derivative on the boundary ($r = a$). The resulting Schrödinger equation

$$(H + \mathcal{L} - E)\psi(1,2) = \mathcal{L}\psi(1,2) \tag{7}$$

then becomes Hermitian within the finite configuration space. In the outer zone (r > a), we neglect the nonlocal effects, which are generally short ranged, and extend the solution into the asymptotic regime by means of standard propagation techniques. Matching to known asymptotic forms determines the scattering parameters such as T matrices, cross sections, and eigenphase sums.

The two linear algebraic methods differ only in their partitioning of PQ space. We invoke the usual Feshbach decomposition [16] in terms of the projection operators P and Q such that

$$\psi = P\psi + Q\psi \tag{8}$$

to derive the following set of coupled equations:

$$(H_{PP} + L_{PP} - E)P\psi + H_{PQ}Q\psi = L_{PP}P\psi, \tag{9}$$

$$(H_{QQ} - E)Q\psi + H_{QP}P\psi = 0. \tag{10}$$

Since Q space contains exclusively short-range terms that vanish at the boundary, the Bloch operator L_{QQ} may be dropped. Formally eliminating $Q\psi$ gives

$$(H_{PP} + L_{PP} + V_{\text{opt}})P\psi = L_{PP}\psi, \tag{11}$$

where

$$V_{\text{opt}} = H_{PQ}(H_{QQ} - E)^{-1}H_{QP} \tag{12}$$

represents the generalized multichannel optical potential. In addition, we employ the integral equations form of the Schrödinger equation

$$P\psi = g_{PP}L_{PP}P\psi \tag{13}$$

with the Green's function defined formally by

$$(H_{PP} + L_{PP} + V_{\text{opt}})g_{PP} = P. \tag{14}$$

In the close-coupling version (CCLA), all states (open and closed) necessary to converge the scattering quantities reside in the first term in Eq. (4). The correlation functions then consist of those products of target states necessary to relax the strong orthogonality constraint. The optical potential, which is employed in the EOLA method, is calculated using the techniques of quantum chemistry. This enables us to calculate the needed H_{QQ} bound-bound matrix elements analytically and to construct the optical potential by solving the (often) large set of algebraic equations implied by Eq. (12) via iterative techniques. If dictated by the physical problem under consideration, we are able to include correlation and polarization effects requiring many thousands of configurations. The optical potential may then be represented as a separable expansion in the short-range correlation functions of Eq. (4). The resultant P-space equations are only marginally more complex than those of standard close-coupling theory [10].

We reduce the three-dimensional, P-space, close-coupling equations to simpler form by invoking a single-center expansion of the bound and continuum orbitals about the molecular midpoint in terms of spherical harmonics Y_{lm} as

$$\varphi_n(\mathbf{r}) = \sum_l \phi_{nlm}(r)Y_{lm}(\hat{\mathbf{r}}), \tag{15}$$

$$F_n(\mathbf{r}) = \sum_l f_{nlm}(r)Y_{lm}(\hat{\mathbf{r}}), \tag{16}$$

where n, l, and m designate a particular electronic state, a channel angular momentum, and the orbital symmetry, respectively. The symmetry of the diatomic implies that the m quantum numbers remain uncoupled

and label the states as $\sigma(m = 0)$, $\pi(m = 1)$, and $\delta(m = 2)$. The bound-state functions $\varphi_n(\mathbf{r})$ come from a multicenter electronic-structure calculation for $H_2{}^+$ using the Gaussian-type orbital (GTO) basis of Ref. [1]. The bound-state energies from this 94-function basis show four-significant-figure agreement with the analytical values of Bates, Ledsham, and Stewart [17]. A detailed comparison of the two approaches appears in Table II of Ref. [1]. Multiplying each side of Eq. (15) by a spherical harmonic and integrating over an angle produces the radial single-center expansion coefficients ϕ_{nlm} for each target electronic state. Substituting Eq. (4) into Eq. (13), using the expansions in Eqs. (15) and (16), and integrating over all target and angular-continuum coordinates convert Eq. (13) into a radial set of coupled integral equations of the general form

$$f_\alpha(r) = G^1_\alpha(r)\delta_{\alpha\beta} - \sum_\beta \int G^0_\alpha(r|r')V_{\alpha\beta}(r')f_\beta(r')dr', \tag{17}$$

where α represents the channel label (n,l,m), G^1_α the regular Coulomb wave function, and G^0_α the channel Coulomb radial Green's function satisfying

$$\left(-\frac{1}{2}\frac{d^2}{dr^2} - \frac{l_\alpha(l_\alpha+1)}{r^2} + 1/r + k^2_\alpha\right)G^0_{l_\alpha}(r|r') = \delta(r-r'), \tag{18}$$

where the channel energy $k^2_\alpha = 2(E - \epsilon_\alpha)$ with E, the total energy, and ϵ_α, a bound-state energy of $H_2{}^+$. Although we have employed a local potential in Eq. (17) for illustrative and pedagogical purposes, the formalism remains equally valid for nonlocal contributions [10] such as exchange and correlation. The regular $G^1_l(r)$ and irregular $G^2_l(r)$ Coulomb functions satisfy the above equation (18) with the right-hand side set to zero. The sums range over an infinite number of channels; however, to obtain a tractable set of equations, we invoke the approximation close-coupling (CC), truncating the number channels at a finite value. The total number of channels consists of the product of the number of electronic states n_s and the number of partial waves n_l included within each state $[n_c = n_s n_l]$. Both quantities must be systematically increased until collisional properties such as the eigenphase sum become converged to within a given tolerance. Since we employ a sufficiently large fixed n_l for all calculations, the symbol n_sCCLA uniquely designates the CC expansion. We then convert this set of coupled integral equations to matrix form by introducing a discrete radial mesh of n_p Gauss-Legendre quadrature points and weights $[(r_i,\omega_i) \mid i = 1, n_p]$. The distribution of the points typically has concentrations in the vicinity of the nucleus $R_n = R/2$. We divide the overall inner radial region [0,a] into N subzones and distribute within each a portion of the points. We designate a mesh as

$$[n_1, n_2, ..., n_N/\bar{r}_0, \bar{r}_1, .., \bar{r}_{N-1}, a], \tag{19}$$

with the ith zone having n_i points and extending in the radial coordinate from $\bar{r}_{i-1}$ to $\bar{r}_i$. We have found that a standard mesh of 60 points and five zones of the form (10,20,10,15,5/0.0,$R_n - 0.5, R_n$+0.5,5.0,10.0,a) generally produces highly accurate results. Applying this quadrature to the functions and integrals in Eq. (17) yields the matrix equation

$$(\mathbf{1} - \mathbf{G}^0\mathbf{U})\mathbf{f} = \mathbf{G}^1, \tag{20}$$

where the matrices have the form

$$[\mathbf{G}^0]_{pq} = G^0_\alpha(r_i|r_j), \tag{21}$$

$$[\mathbf{U}]_{pq} = V_{\alpha\beta}(r_j)\omega_i\omega_j, \tag{22}$$

$$[\mathbf{f}]_p = f_\alpha(r_i), \tag{23}$$

$$[\mathbf{G}^1]_p = G^1_\alpha(r_i), \tag{24}$$

with the term $\mathbf{1}$ representing the unit matrix. The label $p(q)$ designates the composite of a channel and a radial point $[p = (\alpha, i)]$ and the matrix has order $n_c \times n_p$. The $\mathbf{V}$ matrix consists of $n_p \times n_p$ blocks, labeled by the channel indices (α,β); the matrix $\mathbf{G}^0$ is block diagonal with each block a submatrix of order n_p points characterized by a channel α. The set of linear algebraic equations defined by Eq. (20), whose solution gives the channel wave function, is solved by an iterative-variational prescription [18] involving only matrix-vector multiples. In fact, it is possible to reduce the computational and storage costs even further by recognizing the quasiseparable nature of the Green's function for a radial potential. This enables us to express the results of the matrix-vector multiples without actually constructing the matrix and to cut the computational cost by one power in the number of grid points. The local coupled differential equations in the external region ($r > a$) are solved by a Light-Walker [19] RM propagation scheme. We extract the resonance widths and positions from a Breit-Wigner fit [20] of the total eigenphase sum as a function of incident electron energy. On the other hand, in the EOLA, we treat only the open channels in P space and place both orthogonality relaxing and explicit correlation-polarization terms in Q space. The optical-potential construction arises from a two-electron quantum chemistry program as described in earlier publications [10], while the P-space part is handled by the same techniques as described above for the CC linear algebraic method. A detailed description of the GTO bases and of the convergence studies resides in Ref. [1].

The above multichannel integral equations approach for scattering also applies for finding the bound states of the two-electron H_2 molecule. To proceed, we require that the entire two-electron wave function be closed in all expansion channels. A closed channel ($k^2_\alpha < 0$) asymptotically exhibits an exponentially decaying solution

$$f_\alpha(r) \sim \exp(-\kappa_\alpha r), \tag{25}$$

where $\kappa_\alpha = |k_\alpha|$ in all channels. Therefore, by closing

the channels, we convert to an eigenvalue problem [21] whose solution exists only at a discrete set of allowed values of E. These values represent the bound energies of the composite system. Sams and Kouri [22] showed that at these discrete energies E_i, the determinant of the matrix $\mathbf{M}$ defined by

$$\mathbf{M}(E) = \mathbf{1} + \mathbf{G}^2\mathbf{V}\mathbf{f}, \tag{26}$$

vanishes [det$\mathbf{M}(E_i)$=0]. Therefore, by iteratively searching for the values of the energy that satisfy this condition, bound-state eigenvalues result.

In the RM approach, we formally solve Eq. (1) by the prescription

$$\mathcal{R}(E) = \sum_k \frac{\omega_k \omega_k^T}{\varepsilon_k - E}, \tag{27}$$

which defines the inverse of the logarithmic derivative matrix of the solution vector on the boundary ($r = a$). The reduced width amplitudes ω_k represent projections of the RM eigenvectors with eigenvalues ε_k onto the channel states ϕ. The target and correlation functions are expanded in Slater-type orbitals (STO's) centered on the atoms while the continuum functions are represented by a composite of nuclear-centered STO's and numerical orbitals about the center of gravity of the molecule. These numerical functions, which are constrained to be orthogonal to the bound-state orbitals, solve a model Schrödinger equation typically based on the spherically symmetric part of the static potential. Diagonalization of the operator $H+\mathcal{L}$ in the inner region yields the reduced width amplitudes and therefore the R matrix from Eq. (15). The local coupled equations in the external region are solved by an RM propagator [23] and an accelerated Gailitis asymptotic expansion [24]. With this brief description of the techniques in hand, we embark upon a presentation of the results of the various calculations.

Our main focus centers on autoionizing states of the composite H_2 system. These resonance states always consist of at least two electronic channels: (i) an upper closed channel that temporarily forms a doubly excited state of the compound system and (ii) a lower open channel, coupled to the upper state, that allows the electron to escape. The actual situation in electron scattering from H_2^+ presents a more complicated picture with strong coupling among both electronic states and partial waves. To gain some insight into the general problem, we consider a simple Huck model involving only two channels of the form [25]

$$\left[\frac{d^2}{dr^2} - U_{00}(r) + k_0^2\right] f_0 - U_{01}(r) f_1(r) = 0, \tag{28}$$

$$\left[\frac{d^2}{dr^2} - U_{11}(r) + k_1^2\right] f_1 - U_{10}(r) f_0(r) = 0, \tag{29}$$

where $U_{ij}(r) = 2V_{ij}(r), k_0^2 = 2E, k_1^2 = k_0^2 - \Delta E, E$ is the total energy, and ΔE is the excitation energy. All the potentials represent square wells or barriers of width r_w and constant strength U_{ij}. We emphasize that these autoionizing resonances arise from the coupling of at least two electronic channels. Therefore, simple one-channel resonance or virtual state formulas will generally be inadequate, especially in cases of strong coupling. However, as shown by Feshbach [16], the Breit-Wigner form of the eigenphase sum does apply in characterizing the resonant behavior. With the basic formalism established, we now present the results of our calculations.

III. RESULTS AND DISCUSSION

We divide this section into three major parts. In Sec. III A, we present results for the Huck two-channel problem in order to illustrate basic autioionizing resonance behavior. Sections III B and III C treat electron scattering from H_2^+, demarcated by the total symmetry of the two-electron wave function. We first concentrate on the Σ symmetries by presenting highly converged resonance parameters and then give some additional results for Π symmetries that extend the findings of our previous study [1]. We focus on the width Γ and the position E_r of the autoionizing state with respect to the ground state of H_2^+ as a function of internuclear distance R.

Before launching into the details of these calculations, we briefly describe the general nature of the scattering process. Our interest centers on the autoionizing resonances of the composite H_2 system that arise according to the process

$$e^- + H_2^+ \Rightarrow H_2^* \Rightarrow e^- + H_2^+. \tag{30}$$

We concentrate our attention on the energy regime below the first excited-state threshold. To illustrate this mechanism, we use a two-state model in the $^1\Sigma_g$ total scattering symmetry. The lowest two target states of H_2^+ consist of $1\sigma_g$ and $1\sigma_u$ and the composite two-electron channels have the form $1\sigma_g k\sigma_g$ and $1\sigma_u k'\sigma_u$ in order to preserve the correct total symmetry. The symbols k^2 and k'^2 represent the channel energies. For our choice, the lower channel is open ($k^2 > 0$) while the upper channel is closed ($k'^2 < 0$). The upper channel supports a doubly excited state of H_2 of form $(1\sigma_u^2)$. Were the coupling to the open channel zero, this excited state would be purely bound. However, the coupling to the lower open channel provides a mechanism for the electron to escape, thus giving rise to the resonance. In the vicinity of this doubly excited state, the cross section exhibits a pronounced enhancement corresponding to the temporary trapping of the continuum electron. The degree of this trapping determines the lifetime (τ) of the autoionizing state and, in turn, the observed width ($\Gamma \sim 1/\tau$) of the resonant feature in the cross section or eigenphase sum. This resonant effect arises at a given internuclear separation R for the target H_2^+ system. By varying R, we change the position of the doubly excited state and therefore the position of the resonance. At some point, this position moves below the lower channel threshold ($k^2 < 0$) and the H_2 compound state becomes truly bound. We shall present examples of the above-described behavior for electron scattering from the hydrogen molecular ion and, as an illustration, in the simple Huck model.

A. Huck model

We have tested the LA programs for the Huck problem against several older calculations [25], reproducing the cross sections and resonance parameters to a high degree of accuracy. These comparisons considered both all-open and open-closed channel configurations. Choosing a mesh of 200 Gauss-Legendre points in the region $(0,r_w)$, we obtain cross sections to within better than four significant figures of those of the exactly soluble Huck model and resonance widths and positions to better than 1% agreement with Fels and Hazi [25].

For a representative case, we select r_w= 1 bohrs, ΔE=2.25 Ry, U_{00}=0, U_{01}=0.40, and U_{11} as a potential well (<0). The choice closely resembles an example given by Mott and Massey [26] for a moderate coupling strength. In our case, we also select U_{11} deep enough to bind at least one state at $-E_b$ relative to the upper channel threshold. We then investigate the region below the excitation threshold ($k_1^2 < 0$). If the energy $-E_b$ of the bound state in the upper channel potential lies in the range $0 < k_0^2 < \Delta E$, a distinct resonance signature occurs for scattering energies near $k_0^2 \approx \Delta E - |E_b|$. In the case of no coupling (U_{01}=0), no resonance results as the bound state has no mechanism to reach the continuum. As the coupling increases, the position of the resonance shifts and the width broadens. We observe another behavior more akin to the phenomena presented later in this paper by varying the depth of U_{11} in order to model the effects of changing the internuclear distance in $H_2{}^+$. As the bound state deepens, the resonance energy approaches the lower threshold. When $|E_b|$ exceeds ΔE, all channels become closed, the resonance disappears, and a bound state of the composite two-channel system results. For no coupling, this "crossing" occurs at a depth of 6.98 Ry. However, even a moderate amount of coupling changes the picture. Actually closing both states and performing a search based on Eq. (26), we find the system bound for $|U_{11}| > 6.72$ Ry. For less negative values of the potential, we recover the resonance structure in the eigenphase sum. We approach this crossing from above by noting the trend in the resonance position as $|U_{11}|$ increases. For a value of −6.52, we find the resonance at 0.147 Ry with a width of 0.118 Ry. The uncoupled case yields a bound state in this well of −1.922 Ry, which corresponds to a scattering energy of 0.329 Ry. Thus even moderate coupling has a profound effect on the resonance parameters. The behavior of the resonance position as a function of the potential strength is given in Fig. 1. We observe that a simple extrapolation of this position yields a crossing point of about −6.70 Ry within better than 1% of the bound-state results. For the higher strengths, the width becomes much larger than the position. For example, at $U_{11} = -6.66$, the position is at 0.035 Ry and the width is 0.068 Ry. However, the Breit-Wigner (BW) form still provides a valid fit. This arises for two reasons. First, as we noted above, no formal obstacle impedes the application of the BW form in this regime as no explicit assumption pertains as to the relative strength of position and width [16,26]. Second, no numerical obstacle prevents the exercise of this fit as the best root-mean-square error

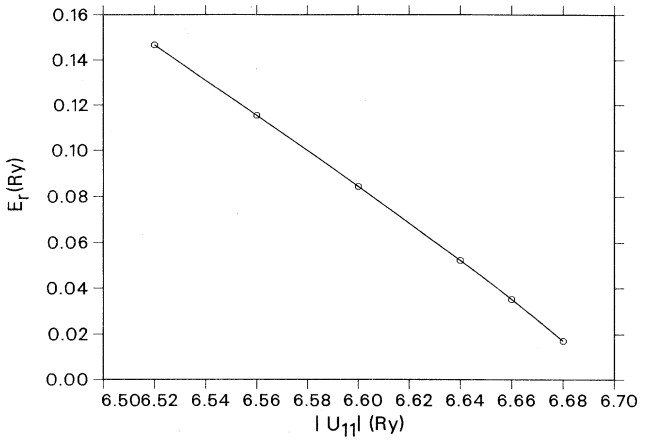

FIG. 1. Position of the autoionizing resonance E_r as a function of potential strength U_{11} for the two-channel Huck problem.

occurs for a cluster of points in close proximity to the resonance position. Having established this trend for a simple model, we now investigate the more complicated electron-molecule scattering problem.

B. Σ symmetries

We begin our investigation of the Σ resonances with the most extensively studied, the $^1\Sigma_g$. The lowest such resonance corresponds to trapping temporarily the electron in the $1\sigma_u^2$ doubly excited state of H_2. However, before delving into the world of autoionizing states, we explore the bound-state regime in order to gain some insight into the accuracy of the various methods. In the LA approaches, we determine the *ground-state* energy of H_2 by closing all channels and determining the root from the prescription described in Eq. (26). In the CCLA case, the calculation represents a hybrid between restricted and unrestricted techniques [27] since we fix one pair of orbitals (φ_n) as a state of $H_2{}^+$ and allow the other (F_n) to freely vary. Since Q space contains all single and double excitations within the orbital basis, the EOLA approach more closely resembles a standard configuration-interaction calculation. In both cases, an iterative process must be invoked to determine the bound state by varying the energy until reaching a zero of the determinant. The Kolos-Wolniewicz calculations [28] still represent the standard for H_2. For the bound $^1\Sigma_g$ state at the equilibrium separation for $H_2{}^+$ (2 bohrs), they report an energy of −1.638 132 hartree. For a four-state ($1\sigma_g, 1\sigma_u, 1\pi_u^{\pm}$) CCLA, we obtain −1.630 95 hartree, while for seven states (4CC,$2\sigma_g$, $2\sigma_u$,$1\pi_g^+$) we have −1.632 22 hartree. We employ a mesh given by (10,20,10,15,5/0.0,0.5,1.5,5.0,10.0,15.0) and three partial waves in each channel (n_c=3). On the other hand, a 400-configuration EOLA calculation yields −1.636 321 hartree. Therefore, the CCLA can produce high-quality bound-state energies, although the convergence with states proceeds slowly. However, we generally found that

TABLE I. Comparison of widths and positions for the $^1\Sigma_g$ resonance at R=2 bohrs for the following methods: RM, R matrix [5]; EOLA and CCLA as defined in the text; PO1, projection operator [8]; PO2, projection operator [9]; KV, Kohn variational [7]. 7CCLA stands for a seven-state ($1\sigma_g$,$1\sigma_u$,$1\pi_u^{\pm}$, $2\sigma_g$,$2\sigma_u$,$3\sigma_g$) close-coupling calculation with n_l=3 and n_p=60 on a standard mesh.

Method	E_r (eV)	Γ (eV)
7CCLA	5.65	1.33
EOLA	5.38	1.39
RM	5.56	1.38
PO1	5.53	1.36
PO2	5.57	1.32
KV	5.47	1.61

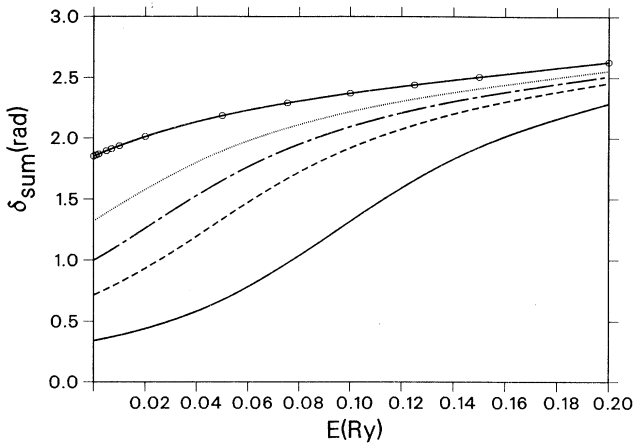

FIG. 2. Eigenphase sum $\delta_{\rm sum}$ in radians as a function of scattering energy E (Ry) and R (bohrs) for $^1\Sigma_g$ symmetry in 7CCLA. The nomenclature for R values is as follows: 2.50, solid line; 2.60, dashed line; 2.65, long-dash–short-dashed line; 2.70, dotted line; 2.80, circled line.

the resonance parameters converged more rapidly than the bound-state energies.

Returning to the autoionizing states, we compare in Table I the positions and widths of the lowest $^1\Sigma_g$ resonance below the first excitation threshold ($1\sigma_u$) for a variety of methods at R=2 bohrs. These include the projection operator techniques of Hazi, Derkits, and Barsley [9] and Hara and Sato [8] as well as Kohn variational procedures [7]. For the RM calculations in this section, we use the results of Shimamura, Noble, and Burke [5] and, in addition, report LA calculations in both approaches. Very good agreement exists among all the methods. We also utilize the results at an internuclear separation of 2 bohrs as a typical example of the convergence in electronic target states. The two-state close-coupling (2CC) calculation consists of the $1\sigma_g$ and the $1\sigma_u$ states; the four-state (4CC) of the 2CC + $1\pi_u^{\pm}$; the six-state (6CC) of the 4CC + $2\sigma_g$ and $2\sigma_u$; the seven-state (7CC) of the 6CC + $3\sigma_g$; and finally, the nine-state (9CC) of the 7CC + $1\pi_g^{\pm}$ with the target states monotonically decreasing in bound energy. The position (width) in eV for n_s = 2, 4, 6, 7, and 9 has values of 6.034 (1.326), 5.895 (1.482), 5.725 (1.454), 5.670 (1.340),

TABLE II. Comparison of H_2 resonance widths and positions as a function of R for various methods for the lowest $^1\Sigma_g$ resonance below the $1\sigma_u$ threshold. The nomenclature is as follows: effective optical-potential linear algebraic, EOLA; n-state close-coupling linear algebraic, nCCLA; and R matrix, RM [5].

R (bohrs)	Method	E (eV)	Γ (eV)
1.4	EOLA	12.57	0.730
	7CCLA	12.75	0.734
	RM	12.80	0.750
2.0	EOLA	5.38	1.39
	7CCLA	5.65	1.33
	RM	5.56	1.39
2.4	EOLA	1.81	1.67
	7CCLA	2.13	2.01
	RM	1.99	1.77
2.5	EOLA	1.05	1.72
	7CCLA	1.27	2.14
	RM	1.23	1.84
2.6	EOLA	0.04	1.75
	7CCLA	0.39	2.14
	RM	0.52	1.90
2.7			

TABLE III. Same as Table II except for the second lowest $^1\Sigma_g$ resonance.

R (bohrs)	Method	E (eV)	Γ (eV)
1.4	EOLA	16.45	0.098
	7CCLA	16.49	0.105
	RM	16.48	0.097
2.0	EOLA	9.926	0.153
	7CCLA	9.963	0.154
	RM	9.946	0.135
2.4	EOLA	6.874	0.180
	7CCLA	6.923	0.168
	RM	6.906	0.150
2.5	EOLA	6.242	0.181
	7CCLA	6.297	0.173
	RM	6.278	0.153
2.8	EOLA	4.610	0.170
	7CCLA	4.679	0.188
	RM	4.656	0.164
3.0	EOLA	3.718	0.216
	7CCLA	3.786	0.199
	RM	3.763	0.169

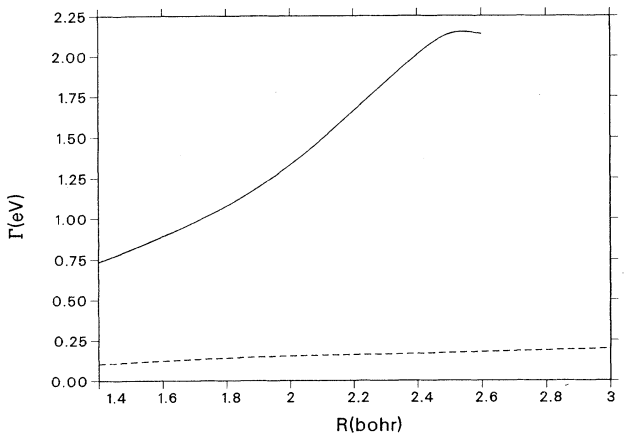

FIG. 3. Width Γ as a function of R for the two lowest resonances in $^1\Sigma_g$ symmetry: solid line, lowest; dashed line, second lowest.

and 5.620 (1.320), respectively. The next two highest sets of target states ($2\pi_u^{\pm}$ and $3\sigma_u$) lie over 0.7 and 2.34 eV, respectively, above the $1\pi_g$ state and play little role in the determination of the low-lying resonance parameters. Fixing the number of states (n_s=7) and varying n_l from 2 to 3 yields positions (widths) of 5.68 (1.32) eV and 5.65 (1.33) eV, respectively. This convergence trend holds for the other total symmetries and internuclear distances. To ascertain better the validity of our three *ab initio* methods (RM, EOLA, and CCLA), we extend the study over a wide range of internuclear distances as shown in Table II. For the CCLA method we used seven states (4CC,$2\sigma_g$,$2\sigma_u$,$3\sigma_g$) with three partial waves per state (n_l=3) and 60 mesh points in the inner zones (a = 15 bohrs) on a standard mesh [see Eq. (19)]. We have varied both the partial wave expansion n_l and the mesh and found convergence at the 5% level for $n_l > 3$ and $n_p > 50$. In general, all three methods agree very well considering the sensitivity of resonance parameters to various collisional variables.

The agreement becomes poorer at larger R. However,

TABLE IV. Same as Table II except for the lowest $^1\Sigma_u$ resonance below $1\sigma_u$ threshold. 4CCLA represents a four-state ($1\sigma_g$,$1\sigma_u$,$1\pi_u^{\pm}$) close-coupling calculation. For 6CCLA, the $2\sigma_g$ and $2\sigma_u$ states are added to the 4CCLA. Both CCLA calculations are with n_l=3 and n_p=60 on the standard mesh.

R (bohrs)	Method	E (eV)	Γ (eV)
1.20	6CCLA	17.09	0.346
	4CCLA	12.25	0.550
1.60	6CCLA	12.19	0.530
	4CCLA	8.51	0.678
2.00	6CCLA	8.47	0.644
	8CCLA	8.46	0.645
	4CCLA	5.80	0.800
2.40	6CCLA	5.75	0.796
2.60	6CCLA	4.69	0.871
2.80	6CCLA	3.80	0.967
3.00	7CCLA	3.04	1.07

at around an R of 2.7 bohrs, the potential-energy curve, marked by the resonance position, crosses the bound-state curve for H_2. To the right of this stabilization point (R_c), the system becomes bound [9,29]. As noted, the actual position of R_c is difficult to ascertain. This stems not so much from the accuracy of the scattering programs, but from the difficulty of defining resonance parameters when the width becomes much larger than the position. In order to investigate the stabilization point in more detail, we present in Fig. 2 the eigenphase sum [$\delta_{\rm sum}(E)$] as a function of scattering energy E and the internuclear distance R. For an R value of 2.5 bohrs, the distinct BW resonance shape appears with an inflection point near the resonance position E_r. In fact, a valuable means of identifying resonances exploits this inflection signature by searching for a change of sign in the second derivative of $\delta_{\rm sum}$ as a function of energy [20]. As R increases, this

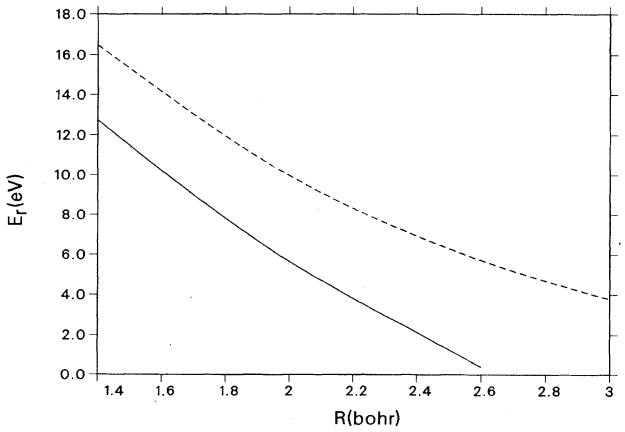

FIG. 4. Same as Fig. 2 except for position.

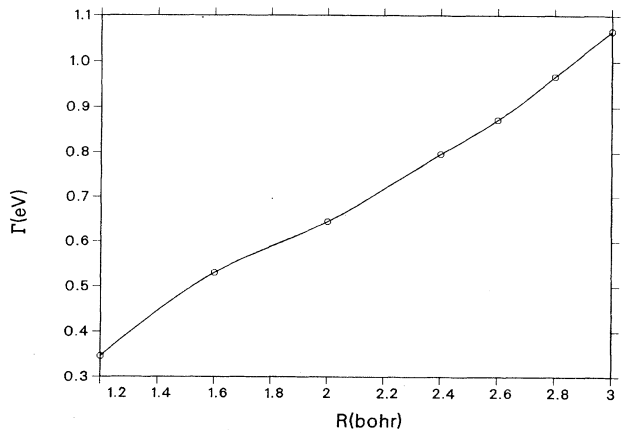

FIG. 5. Width as a function of R for the lowest $^1\Sigma_u$ resonance.

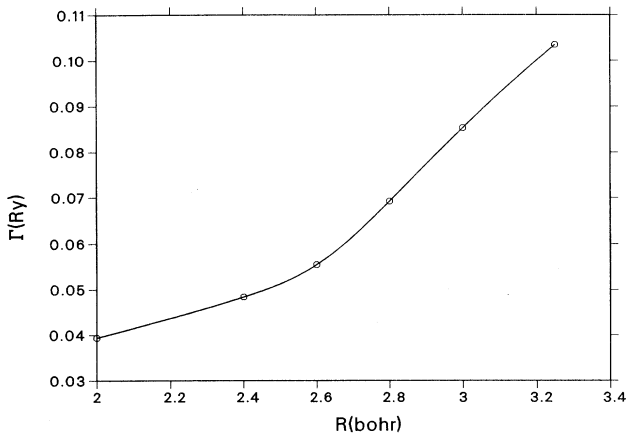

FIG. 6. Width Γ as a function of R for the $^1\Pi_g$ symmetry.

feature disappears ($\sim$ 2.7 bohrs) yielding a simple monotonically rising phase with energy. This behavior can be quantified by fitting to the BW form and extrapolating the resonance position to a zero value, much as was done in the Huck case. A simple extrapolation of the resonance energy yields R_c=2.65 bohrs, in excellent agreement with the RM results [5]. We also note that $\delta_{\rm sum}$ tends to a finite value at E=0, an indication of very strong interchannel coupling. We have not performed bound-state calculations for $R > 2.7$ bohrs since accurate results of comparable quality already exist [29]. Finally, in Table III, we present a similar study of the next highest lying $^1\Sigma_g$ resonance. Again, we note very good agreement among the methods. The results for both resonances are summarized in Figs. 3 and 4.

We now turn our attention to the $^1\Sigma_u$ resonances. In Table IV, we display the widths and positions as a function of R for the lowest $^1\Sigma_u$ resonance below the first excitation threshold. We have extended this case to larger R values due to its importance for other processes [2]. We also show the convergence properties for different numbers of target states with the basic description the same as for the $^1\Sigma_g$. We employ a standard mesh [a=15 bohrs] with n_p=60 and n_l=3 and again note the general trend of the position decreasing and the width growing as R increases. This state has been examined experimentally [11]. However, the data suggested a much larger width, especially beyond R=2 bohrs, than previously predicted by theoretical calculations. Our results support these earlier calculations in obtaining widths well over a factor of 2 lower than the experiment and in excellent agreement with the theoretical findings. As shown in Fig. 5, we do not observe the leveling of the width of Tennyson [30] beyond about 2.6 bohrs. However, we do certainly observe a change in slope in this region, albeit with the width not rising quite so rapidly. This region has difficulties as reported earlier in that the definition of a resonance becomes somewhat ambiguous once the width exceeds the position. The principal contribution omitted from the current formalism is the coupling due to nuclear motion. Further tests will have to be run to determine the effects of this omission.

TABLE V. Widths and positions as a function of R of the lowest resonance of the Π_g symmetry for $e^- + H_2^+$ collisions below the $1\sigma_u$ threshold at the 8CCLA level (n_c =3, n_p=60). Eight target states are included: $1\sigma_g$,$1\sigma_u$,$1\pi_u^{\pm}$,$2\sigma_g$,$2\sigma_u$,$1\pi_g^{\pm}$.

R (bohrs)	E (Ry)	Γ (meV)
2.00	0.6128	3.939(-2)
2.40	0.4056	4.836(-2)
2.60	0.3220	5.543(-2)
2.80	0.2538	6.921(-2)
3.00	0.1927	8.533(-2)
3.25	0.1218	1.035(-1)

C. Π symmetry

Since the $^1\Pi_g$ symmetry plays an important role in dissociative recombination [3], we have extended our previous calculations to larger internuclear separations. We first note two typographical errors in our earlier paper [1]: (i) the position at 1.4 bohrs as given in Table VIII of [1] should read 1.0767 Ry and (ii) the units of energy in Fig. 6 should be hartrees. In Table V, we present the widths Γ and positions E_r as a function of R from 2.0 to 3.25 bohrs. All calculations were performed in the CCLA method for eight target states ($1\sigma_g$,$1\sigma_u$,$1\pi_u^{\pm}$, $2\sigma_g$,$2\sigma_u$,$1\pi_g^{\pm}$) with three partial waves to each channel (n_l=3) and 60 mesh points in the LA zone ($r \leq 15$ bohrs) on a standard mesh. Convergence studies demonstrate that the resonance parameters should be accurate to better than 10%. As indicated in Fig. 6, the width slowly rises as R increases while the position declines. While covering a greater region of importance to dissociative recombination, these results do not appear to substantially change calculations [3] based on extrapolations from previous findings.

ACKNOWLEDGMENTS

Two of us (L.A.C. and B.I.S) acknowledge support of the U.S. Department of Energy through the Theoretical Division at the Los Alamos National Laboratory. Additional funds for this collaboration were provided by NATO Scientific Exchange Grant No. 687/84.

[1] L.A. Collins, B.I. Schneider, and C.J. Noble, Phys. Rev. A **45**, 4610 (1992).

[2] *Dissociative Recombination*, edited by J.B.A. Mitchell and S. Guberman (World Scientific, Singapore, 1989); *Dissociative Recombination*, edited by B.R. Rowe, J.B.A. Mitchell, and A. Canosa (Plenum, New York, 1993).

[3] I.F. Schneider, O. Dilieu, A. Giusti-Sazor, and E. Roueff, Astrophys. J. **424**, 983 (1994).

[4] L.A. Collins, B.I. Schneider, C.J. Noble, C.W. McCurdy, and S. Yabushita, Phys. Rev. Lett. **57**, 980 (1986).
[5] I. Shimamura, C.J. Noble, and P.G. Burke, Phys. Rev. A **41**, 3545 (1990).
[6] J. Tennyson, C.J. Noble, and S. Salvini, J. Phys. B **17**, 905 (1984); J. Tennyson and C.J. Noble, *ibid.* **18**, 166 (1985); J. Tennyson, C.J. Noble, and P.G. Burke, Int. J. Quantum Chem. **24**, 1033 (1986); J. Tennyson, J. Phys. B **20**, L375 (1987).
[7] H. Takagi and H. Nakamura, J. Phys. B **13**, 2619 (1980); Phys. Rev. A **27**, 691 (1983); J. Chem. Phys. **84**, 2431 (1986).
[8] S. Hara and H. Sato, J. Phys. B **17**, 4301 (1984); **19**, 2611 (1986).
[9] A.U. Hazi, C. Derkits, and J. Barsley, Phys. Rev. A **27**, 1751 (1983).
[10] L.A. Collins and B.I. Schneider, Phys. Rev. A **24**, 2387 (1981); B.I. Schneider and L.A. Collins, *ibid.* **28**, 166 (1983); **27**, 2847 (1983).
[11] C.J. Latimer, K.F. Dunn, N. Kouchi, M.A. McDonald, V. Srigengan, and J. Geddes, J. Phys. B **26**, L595 (1993).
[12] E. Charron, A. Giusti-Suzor, and F.H. Mies, Phys. Rev. Lett. **71**, 692 (1993); Phys. Rev. A **49**, R641 (1994).
[13] *Atoms in Intense Fields*, edited by M. Gavrila (Academic, New York, 1992); J. Shertzer, A. Chandler, and M. Gavrila (unpublished).
[14] B.I. Schneider and L.A. Collins, Comput. Phys. Rep. **10**, 50 (1989); L.A. Collins and B.I. Schneider, Phys. Rev. A **27**, 101 (1983).
[15] C. Bloch, Nucl. Phys. **4**, 503 (1957).
[16] H. Feshbach, Am. Phys. (N.Y.) **5**, 357 (1958).
[17] D.R. Bates, K. Ledsham, and A.L. Stewart, Proc. Phys. Soc. London Sect. A **246**, 28 (1953).
[18] B.I. Schneider and L.A. Collins, Comput. Phys. Commun. **53**, 381 (1989).
[19] J.C. Light and R.B. Walker, J. Chem. Phys. **65**, 4272 (1976).
[20] J. Tennyson and C.J. Noble, Comput. Phys. Commun. **33**, 421 (1989).
[21] P.G. Burke and M.J. Seaton, in *Methods of Computational Physics*, edited by B. Alder, S. Fernbach, and M. Rotenberg (Academic, New York, 1971), Vol. 10, p. 50.
[22] W.N. Sams and D.J. Kouri, J. Chem. Phys. **52**, 4144 (1970).
[23] K.L. Baluja, P.G. Burke, and L.A. Morgan, Comput. Phys. Commun. **27**, 299 (1982); L.A. Morgan, *ibid.* **31**, 419 (1984).
[24] C.J. Noble and R.K. Nesbet, Comput. Phys. Commun. **33**, 399 (1984).
[25] R.J. Huck, Proc. Phys. Soc. London Sect. A **70**, 369 (1957); R.K. Nesbet, Phys. Rev. **179**, 60 (1969); M.F. Fels and A.U. Hazi, *ibid.* **5**, 1236 (1972); C.W. McCurdy and T.N. Rescigno, *ibid.* **20**, 2346 (1979).
[26] N.F. Mott and H.S.W. Massey, *The Theory of Atomic Collisions* (Oxford University Press, Oxford, 1965).
[27] A. Szabo and N.S. Ostlund, *Modern Quantum Chemistry* (McGraw-Hill, New York, 1989).
[28] W. Kolos and L. Wolniewicz, J. Chem. Phys. **43**, 2429 (1965); **45**, 509 (1966).
[29] S.L. Guberman, J. Chem. Phys. **78**, 1404 (1983).
[30] As reported in Ref. [11].